THE ASTROPHYSICAL JOURNAL, 449:900–908, 1995 August 20

SPECTROSCOPIC *EUVE* OBSERVATIONS OF THE ACTIVE STAR AB DORADUS

SLAVEK M. RUCINSKI
Institute for Space and Terrestrial Science and York University, 4850 Keele Street, Toronto, Ontario, Canada M3J SK1
ROLF MEWE
Space Research Organization Netherlands (SRON), Sorbonnelaan 2, NL 3584 CA Utrecht, The Netherlands
JELLE S. KAASTRA
Space Research Organization Netherlands (SRON), Sorbonnelaan 2, NL 3584 CA Utrecht, The Netherlands
OSMI VILHU
Observatory and Astrophysics Laboratory, Box 14, FIN-00014 University of Helsinki, Finland
AND
STEPHEN M. WHITE
Department of Astronomy, University of Maryland, College Park, MD 20742
Received 1994 July 8; accepted 1995 February 27

ABSTRACT

We present observations of the pre–main-sequence, rapidly rotating (0.515 day) late-type star, AB Doradus (HD 36705), made by the *Extreme Ultraviolet Explorer* (*EUVE*) satellite. A spectrum from 80 to 700 Å with a resolution $\Delta\lambda \approx 0.5$–2 Å was accumulated between 1993 November 4–11, with an effective exposure time of about 40 hours. No obvious EUV flares were detected during the observation. The data constrain the coronal temperature structure between several 10^4 K up to roughly 2×10^7 K through a differential emission measure analysis using the optically thin MEKA plasma model. The resulting differential emission measure (DEM) distribution shows: (1) dominant emission from plasma between about 2×10^6 and 2×10^7 K, which may show a substructure with two components around 3×10^6 and 10^7 K; (2) very little emission from plasma between 10^5 and 2×10^6 K; and (3) emission from plasma below about 10^5 K. If solar photospheric abundances are assumed, then the *formal* DEM solution also requires the presence of a strong high-temperature component (above about 3×10^7 K) in order to explain the strong continuum emission below about 150 Å. We believe that this component of the solution is not physical: it is not present in the solution if we assume lower iron abundance, or if there is significant resonance scattering in some of the stronger (mainly iron) spectral lines with subsequent photon absorption in the lower, dense atmosphere. Finally, the DEM analysis gives a best-fit value for the interstellar hydrogen column density of $N_H = (2.4 \pm 0.5) \times 10^{18}$ cm^{-2}.

Subject headings: stars: activity — stars: coronae — stars: individual (AB Doradus) — stars: late-type — stars: pre–main-sequence — ultraviolet: stars

1. INTRODUCTION

Since its identification as a flaring *Einstein* X-ray source (Pakull 1981), AB Doradus (HD 36705) has been one of the most frequently observed active late-type stars. Its particular importance is due both to its very short rotation period (0.515 day) for its spectral type of K0–K2 IV–V, and to its proximity to the Sun (distance 20–30 pc; Rucinski 1985; Innis, Thompson, & Coates 1986). The discoveries of a strong lithium absorption line in its spectrum (Rucinski 1982, 1985) and of kinematic properties characteristic of the Pleiades group (Innis et al. 1986) have established the star as one of the nearest pre–main-sequence objects in the solar neighborhood, with an inferred age of 10^{6-7} years.

AB Doradus is easily detected in all spectral bands from the X-rays to radio. Following the *Einstein* observations, Collier Cameron et al. (1988) using the *EXOSAT* ME detector found a hot thermal corona. The spectral information in this observation was scant but the whole emission in the low (0.05–2 keV) and medium (1–10 keV) energy ranges of *EXOSAT* could be explained by a one-component plasma at about 2×10^7 K with an emission measure of about 2.3×10^{53} cm^{-3} (for an assumed distance of 25 pc). X-ray flares were observed with a rate of about one per 0.5 day stellar rotation. The same rate was observed during an extensive multifrequency campaign of coordinated observations extending from X-rays (*Ginga* satellite) to radio (3 cm, Parkes radio telescope) conducted by Vilhu et al. (1993). The *ROSAT* X-ray all-sky survey observations of AB Dor (Kürster, Schmitt, & Fleming 1992) obtained over a period of more than a month showed erratic variability with very weak rotational modulation.

The corona of AB Dor is also practically always visible in the radio as nonthermal emission at frequencies as low as 843 MHz (Beasley & Cram 1993), and as high as 8.6 GHz (Vilhu et al. 1993). At 6 cm, the star has often shown a clear and regular rotational modulation (Lim et al. 1992, 1994, and references therein). Spectroscopic optical studies of Collier (1982) and Vilhu, Gustafsson, & Edvardson (1987) gave $v \sin i = 100 \pm 5$ km s^{-1} and a radial velocity constant to ± 2 km s^{-1}.

The chromospheric and transition-region emission of AB Doradus was analyzed with the *IUE* satellite by Rucinski (1985). The overall level of emission was found to be very high and the star seemed to be rather uniformly covered by active regions at that time. This result, together with the hot coronal component derived by Collier Cameron et al. (1988) from the

EXOSAT ME spectra suggested an obvious follow-up with the *EUVE* satellite whose spectral range probes the region of temperatures between 10^5 and 10^7 K.

AB Dor forms a wide binary with the young rapidly rotating M-type dwarf Rst 137B (Vilhu & Linsky 1987; Vilhu et al. 1989). Since this secondary is bolometrically about 60 times fainter than AB Dor, and the "saturation" phenomenon (Vilhu & Walter 1987) should apply to Rst 137B as it does to AB Dor, we do not expect Rst 137B to contaminate significantly the EUV spectrum of AB Dor. Thus, AB Dor can be probably treated as an "effectively single" star, when the stars cannot be angularly separated, as in this study.

We describe the *EUVE* observations in § 2. Section 3 describes the spectral analysis and the differential emission measure modeling (DEM) method, gives the DEM results and discusses the high-temperature component in DEM. Section 4 contains conclusions and a comparison with *EUVE* observations of nine other cool stars.

2. OBSERVATIONS

The *Extreme Ultraviolet Explorer* observations of AB Dor were obtained during the first round of the Guest Observer Program (EGO) on that satellite. The observations started on 1993 November 4 and continued for 14 rotations of the star until 1993 November 11 (JD 2449295.94 – 2449302.74). The data were collected in three spectroscopic bands, SW: 80–180 Å, MW: 150–350 Å, and LW: 300–700 Å, as well as with the Deep Sky Survey (DSS) imager (60–150 Å). Results of a time variability analysis to study rotational modulation in the EUV spectra, in the DSS channel and from extensive optical and radio ground-based supporting observations will be presented by White et al. (1995a). An observation of AB Dor with the *ASCA* X-ray satellite, obtained during our *EUVE* observations (White et al. 1995b) helped to constrain our interpretations (see § 3.4). AB Dor did not show any major flares in the EUV, and was in a low-radio-flux state. Optical monitoring (White et al. 1995a) showed no flaring except during a brief period amounting to no more than 5% of the *EUVE* observation, so that time-averaging of our spectra should result in data representative of the quiescent state of AB Dor with no significant contamination from flare emission.

The *EUVE* data were reduced at the Center for EUV Astrophysics in Berkeley, using IRAF and the newly released calibration data set "egodata 1.8.1," paying special attention to the problem of background subtraction. The effective exposure times for our spectra were about 40 hours (155700, 143012, and 145139 s in SW, MW and LW, respectively). The original two-dimensional 2048 × 2048 pixel images containing the spectra, whose spectral resolution was oversampled about 7×, were rebinned by a factor of 2. Then, the two-dimensional background was determined within a strip of 128 rebinned pixels wide along the spectrum. The background was then smoothed and interpolated in both directions. The spectra were extracted using "slits" which were 11, 9, and 7 (rebinned) pixels in width in the SW, MW and LW channels, respectively.

Small-scale distortions in the microchannel plate detectors result in semi-regular spatial variations in the sensitivity of some 10%–20% (see EGO Center User's Guide), leading to an increased uncertainty estimate. We allow for this variation by adding an error of 15% of the signal in both the background and the net observed spectrum on top of the uncertainty expected purely from count-rate statistics.

By virtue of the use in this analysis of the new EGO data set "egodata1.8" implemented in 1994 January, it was not necessary to perform an extensive wavelength recalibration as was required for earlier data based on previous reference data sets (for details see Mewe et al. 1995a, hereafter MKSOA95; detailed line identifications can be found in the tables in the Appendix of their paper). We checked the new calibration by doing a preliminary differential emission measure analysis in each of the three wavelength bands and compared the model spectrum with the observed one. A preliminary spectral fit established that only in the SW there was a systematic offset in the line centroids: the observed wavelength values were all 0.25 Å higher than the theoretical ones, so we shifted the SW data set accordingly.

The effective areas for the first and higher grating orders were implemented in our analysis using the EGO calibration data set. The assumption of a Gaussian profile for the instrumental response function with the nominal resolution (FWHM) was found to be sufficient for all analyzed lines; there was no need to introduce a Voigt profile, as was needed in the analysis of α Cen which has a much higher signal-to-noise ratio (MKSOA95).

For the final spectral analysis, we rebinned the spectra into wavelength intervals of 0.25, 0.5, and 1.0 Å for the SW, MW, and LW, respectively. This binning corresponds to about 4 original pixels and ensures that the number of counts (source plus background) is large enough in each bin so that the assumption of Gaussian statistics, as implicity assumed in the χ^2 statistics, is warranted. Typically all bins in the *raw* data contain 50–100 background counts. Such rebinned spectra over-sample the resolution of the *EUVE* spectrographs by a factor of 2.

The choice of spectral ranges for the spectral analysis was dictated mainly by the background level and by contamination from second- and third-order lines in the MW and LW ranges. We exclude from the analysis (1) pixels near the detector edges which had a high background, (2) pixels that overlapped in different wavelength bands where the efficiency cross-calibration was uncertain, and (3) pixels with uncertain efficiencies for higher orders. We consequently exclude LW data longward of 510 Å because of the presence of many second- and third-order lines, and MW data shortward of the aluminum *L*-edge at ~170 Å and longward of the corresponding second order at ~340 Å. This leaves in total 420 wavelength bins between 76–181 Å for the SW band, 336 bins between 172–340 Å for the MW, and 170 bins between 340–510 Å for the LW. The three spectral bands, covering in total 926 bins, are used jointly in the spectral analysis discussed in § 3.

The spectra expressed in total accumulated counts, corrected for the background are shown for the three bands in Figures 1 to 3. For the stronger lines we indicate the ions from which they originate (see also Table 1 which gives the intensities of these lines expressed in predicted model counts). In cursory examinations of the spectra, we note that, in addition to the prominent lines in the SW band, we see a relatively strong continuum between about 80 and 150 Å. The noise level in the vicinity of the helium lines (e.g., He II at 304 Å line, see Fig. 2) is relatively high, even after background subtraction, due to strong geocoronal contributions in these lines. This is because AB Dor is situated at a high ecliptic latitude (−87°) and therefore on average the angle between the pointing direction of the telescope and the bright Earth is smaller than for most other sources, leading to relatively more scattered geocoronal light entering the detectors.

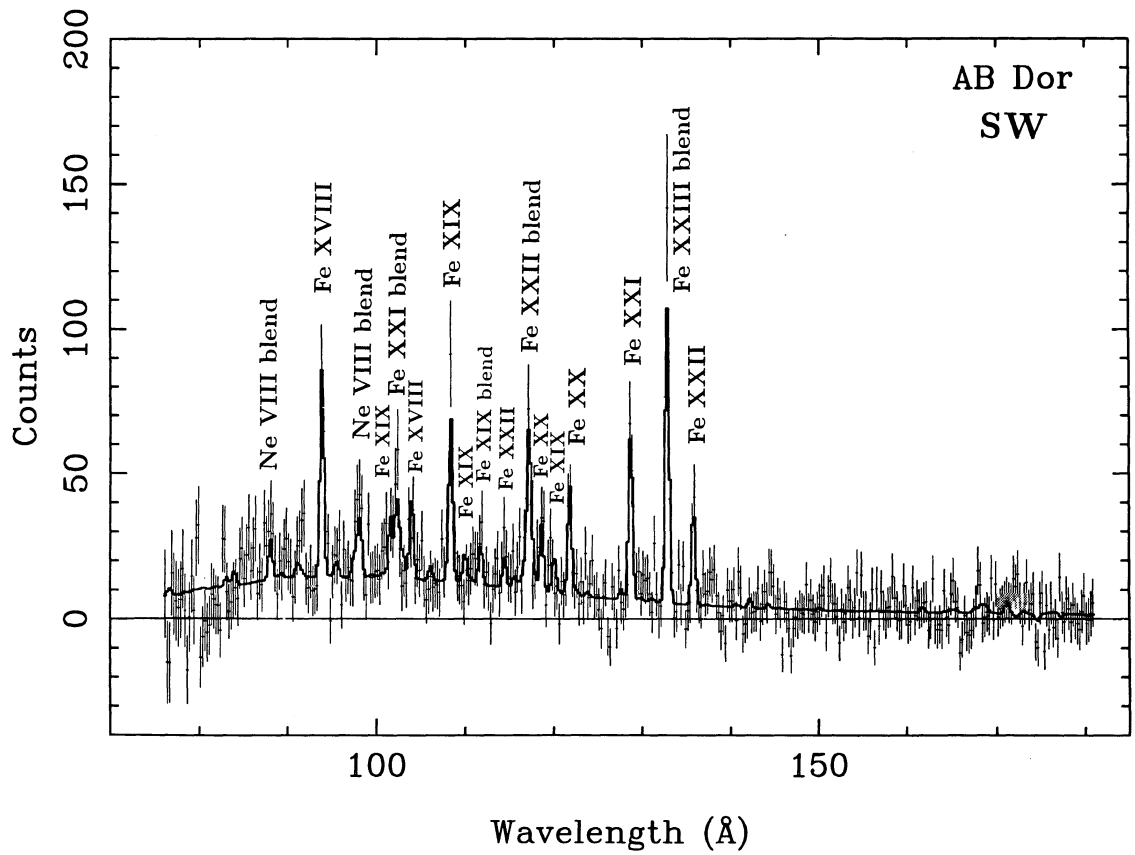

FIG. 1.—*EUVE* background-corrected spectrum of AB Dor. Shown is the binned spectrum (see § 2) for the SW passband. The observed spectrum is shown with the uncertainties on the observed number of counts. The 1 σ error bars include the effects of statistical Poisson photon and background noise as well as systematic errors, as described in the text. The best-fit spectrum, of which the differential emission measure distribution $\boldsymbol{D}(T)$ is plotted in Fig. 4, is shown by the thick solid line. Several prominent lines (which are listed in Table 1) are indicated by the ions from which they originate.

3. SPECTRAL ANALYSIS

3.1. *Assumptions*

To analyze the *EUVE* spectrum, we calculated isothermal equilibrium spectra utilizing a spectral mode which has evolved from the well-known and widely used optically thin plasma code developed by Mewe and coworkers (e.g., Mewe, Gronenschild, & van den Oord 1985; Mewe, Lemen, & van den Oord 1986), and implemented in the X-ray spectral data analysis package XSPEC (maintained by the High Energy Astrophysics Science Archive Research Center of NASA) as the modeling code "MEKA" (see Kaastra & Mewe 1993; Mewe & Kaastra 1994). In this study we used the newly developed SPEX code (see Kaastra & Mewe 1993; Mewe & Kaastra 1994), which is augmented with spectral lines between 300–2000 Å from Landini & Monsignori Fossi (1990) but with wavelengths and excitation rates modified in several places. The treatment of continuum emission has also been improved, using photoionization rates based upon Verner et al. (1993).

Each of the calculated spectra is modified by interstellar absorption using the absorption cross sections of Rumph, Bowyer, & Vennes (1994), and convolved with the instrument response, taking into account the latest updates on the effective areas, binning, response, and resolution characteristics of these instruments (see *EUVE* Guest Observer Handbook, NRA 93-OSSA-X, version 1993 June 4). In the analysis we assume a source distance $d = 25$ pc, and initially we adopt solar photospheric abundances from Anders & Grevesse (1989). When calculating interstellar absorption we use an interstellar hydrogen column density of $N_{\rm H} = 2.4 \times 10^{18}$ cm^{-2} which followed from a best-fit [$N_{\rm H} = (2.4 \pm 0.5) \times 10^{18}$ cm^{-2}] to the data, with adopted abundance ratios He I/H I = 0.1 and He II/H I = 0.01. However, the final results are not very sensitive to these ratios.

3.2. *DEM Modeling Method*

In our analysis, we follow the procedure described by MKSOA95, where details of the line identifications and the differential emission measure (DEM) modeling technique are given. Here we give a brief description.

In a stellar corona which is assumed to be optically thin the emitted EUV spectrum is not a unique function of one single temperature, but instead is determined by a linear combination of isothermal plasmas and described in terms of the "differential emission measure" (DEM) distribution over the range of temperatures for which the instrument is sensitive. Under the optically thin assumption all plasma temperature components can be considered to be observed as emitted, regardless of where they occur on the stellar disk. The DEM function, defined to be $\boldsymbol{D}(T) = n_e n_{\rm H} dV/d \log T$, is the weighting function which measures how strongly any particular temperature contributes to the observed spectrum (T is the electron temperature, n_e is the electron density, $n_{\rm H}$ is the hydrogen density, and V is the plasma volume). The observed spectrum is interpreted as a statistical realization of a linear combination of isothermal spectra. We implicitly assume that

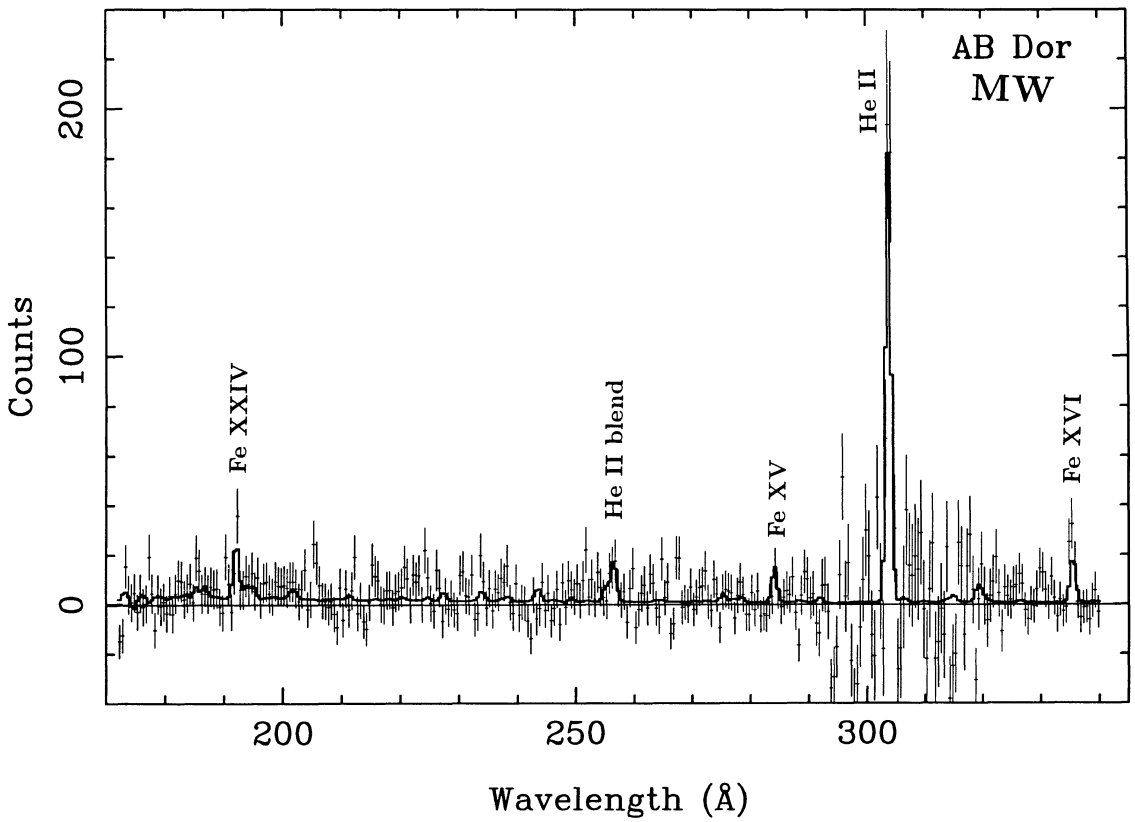

FIG. 2.—*EUVE* background-corrected spectrum of AB Dor. Same as in Fig. 1, but for the MW passband.

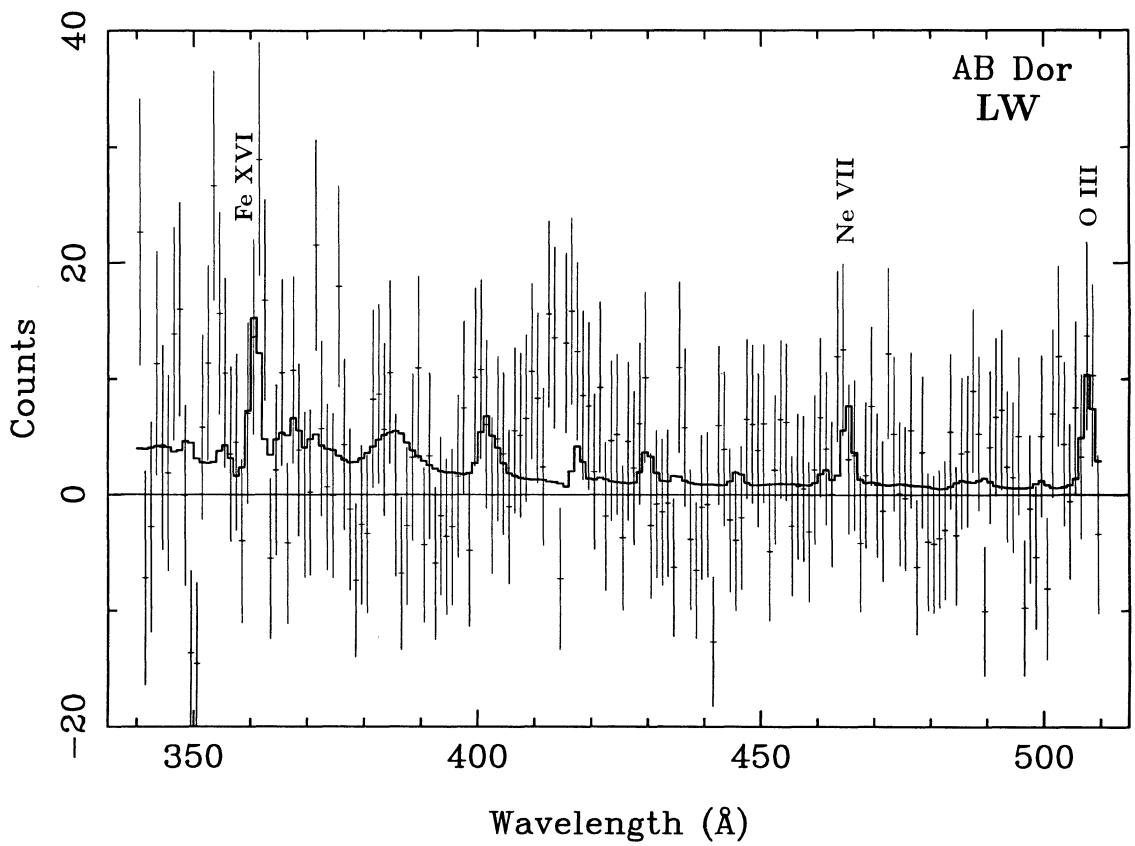

FIG. 3.—*EUVE* background-corrected spectrum of AB Dor. Same as in Fig. 1, but for the LW passband.

all plasma components are in thermal ionization equilibrium, thus ignoring any transient effects, and we ignore effects associated with the plasma density. Deviations from the optically thin model caused by possible resonance scattering effects are discussed later on. The shape of the DEM distribution is derived from the observed emission line *and* continuum fluxes. We stress here that it is important that we include the continuum in our analysis since it is the line-to-continuum ratio that can provide important information on the abundances (in particular the [Fe/H] ratio) and line scattering effects.

We now address the inversion problem of recovering the DEM distribution $\boldsymbol{D}(T)$ from the observed spectrum. Let an isothermal plasma of temperature T emit a spectrum, incorporating interstellar absorption, instrumental efficiencies, and instrumental smoothing, represented by $f(\lambda_i, T_j)$ in wavelength bins $i = 1, \ldots, N$ and temperature intervals $j = 1, \ldots, M$ where $f(\lambda_i, T_j)$ is the plasma emissivity per unit $n_e n_{\rm H}$ as given by the MEKA code. For a composite plasma with temperatures ranging from T_1 up to T_M, the net expected spectrum $g(\lambda_i)$ is given by

$$g(\lambda_i) = \int f(\lambda_i, T)\, n_e\, n_{\rm H}(T)\, dV(T)$$

$$\approx \sum_{j=1}^{M} f(\lambda_i, T_j)\, \boldsymbol{D}(T_j)\, \Delta\log\,(T)\,. \qquad (1)$$

We use a grid of 41 logarithmically spaced temperatures between 0.001–10 keV (1.16×10^4–1.16×10^8 K). Throughout this paper, the emission measure is plotted as $\boldsymbol{D}(T)\,\Delta\log T$, with $\Delta\log T = 0.1$. In this way the total emission measure in any temperature range can be obtained by summing the values of $\boldsymbol{D}(T)\,\Delta\log T$ of each temperature bin in this range as given in Figures 4 and 5.

In the past we have often applied the Withbroe-Sylwester iterative technique (e.g., Sylwester, Schrijver, & Mewe 1980) originally proposed to interpret high-resolution solar X-ray spectra, and subsequently extended by Lemen et al. (1989) to analyze *EXOSAT* transmission-grating spectra of late-type stars. Here, we use another inversion technique as discussed by Craig & Brown (1986), Press et al. (1992), and described in detail in MKSOA95.

The inversion problem (equivalent to a Fredholm equation of the first kind) is ill-posed and solutions tend to show large, unphysical oscillations. We therefore apply a second-order regularization ("smoothing"), i.e., of all solutions which are consistent with the data we select the DEM which has the smoothest second derivative. The wavelength range covered by *EUVE* contains only a few weak lines from plasma at temperatures exceeding 1.5–2.0×10^7 K. The maximum in the continuum spectrum moves shortward of the observed wavelength range for temperatures exceeding roughly 3×10^6 K, while the associated long-wavelength component in the *EUVE* range is rather insensitive to changes in the temperature. Therefore, the continuum from plasma with temperatures exceeding roughly 3×10^6 K can only yield evidence that plasma at these temperatures is present, but cannot yield more detailed information on the actual temperature distribution. Because no sufficiently strong temperature-constraining lines

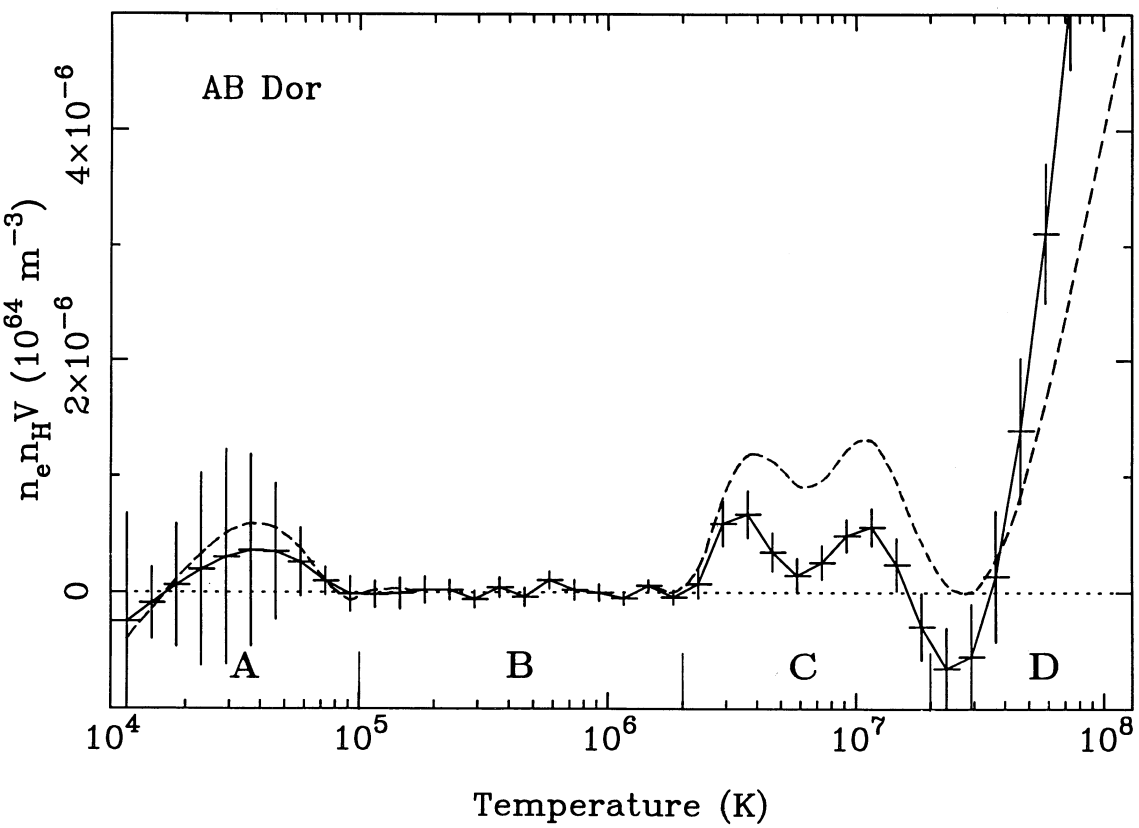

FIG. 4.—Differential emission measure (DEM) curve $\boldsymbol{D}(T)\,\Delta\log T$ for AB Dor corresponding to the best-fit theoretical spectrum shown in Figs. 1–3, based on standard solar abundances (*solid line with error bars*) and the DEM derived for the case with the iron abundance reduced by a factor of 3.3 (*dashed line*). The quantity plotted along the vertical axis is the product of electron density, hydrogen density, and plasma volume per logarithmic temperature bin $\Delta\log T = 0.1$.

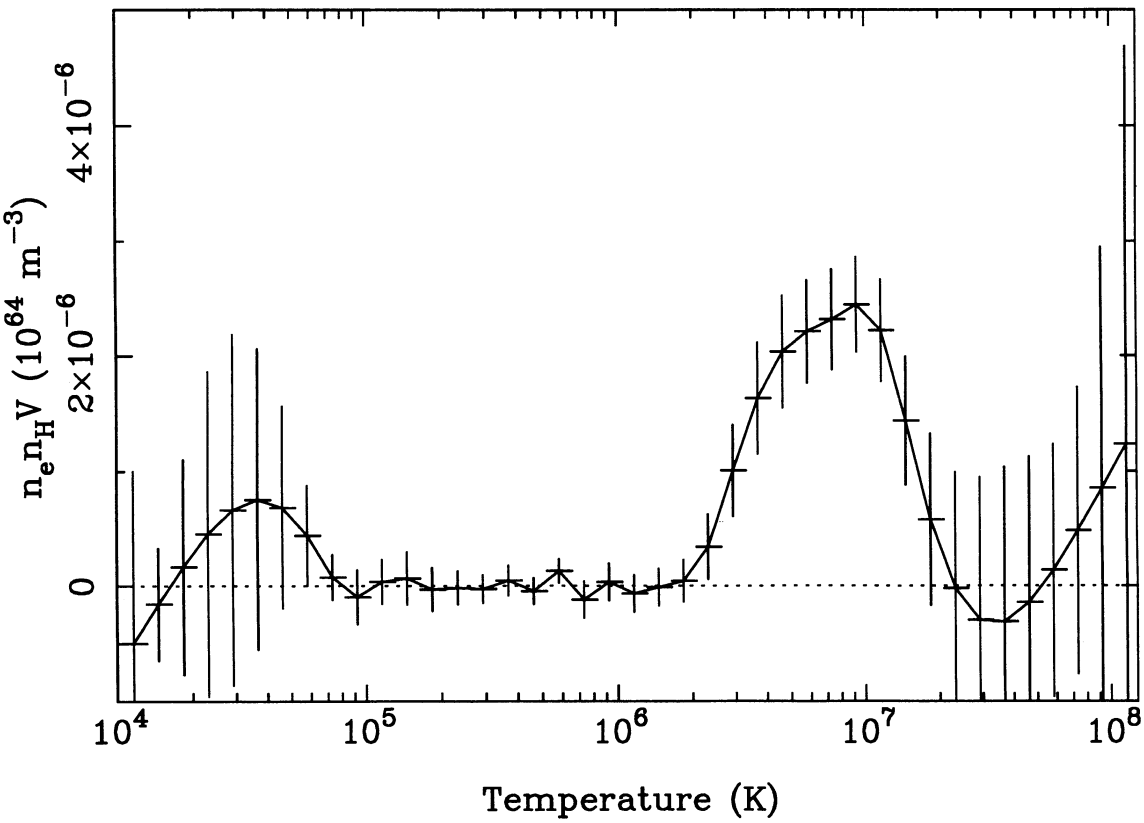

FIG. 5.—Differential emission measure (DEM) curve $D(T)$ $\Delta\log T$ for AB Dor corresponding to the best-fit theoretical spectrum shown in Figs. 1–3 based on abundances for the *ASCA* fit model with the iron abundances 0.133 times solar (i.e., the high-temperature component of the *ASCA* model, see § 3.4).

are observed from plasma with temperatures exceeding about 1.5–2.0 × 10^7 K, the temperature structure of plasma with these temperatures cannot be determined with *EUVE* data: the DEM analysis will register the need for a hot component to exist, but the second-order smoothing results in a straight line reflecting the total continuum emission strength rather than the true temperature structure or even the true integrated emission measure (this is discussed in more detail in § 3.4.).

The errors of the DEM are derived as described by MKSOA95; they reflect the (weighted) statistical uncertainty of the signal of each spectral bin contributing to the DEM in a particular temperature interval. In the temperature region of 10^5–10^7 K the errors in adjacent temperature intervals are nearly statistically independent because the presence or absence of many spectral lines in the *EUVE* band constrains the DEM and its errors. Outside this range the *EUVE* data give fewer constraints: essentially only the He II 304 Å line at lower temperatures, and the SW continuum at higher temperatures. Here the errors are strongly correlated and only the integrated DEM with its formal error gives some indication of the significance of a temperature component. Consequently the shape of the DEM in these regions cannot be determined uniquely from the *EUVE* data, and the solution presented in Figures 4 and 5 is only one of the many possible solutions which are all statistically acceptable.

We stress that the regularization method is not an iterative procedure. An iterative method requires an initial DEM distribution and, depending on the details of the distribution, the iteration may not converge to the true solution, but instead may yield a solution corresponding to, e.g., a local minimum in the χ^2-space. This problem is avoided by the inversion method we use. We have already applied this method to the *EUVE* spectra of eight other cool stars (MKSOA95; Schrijver et al. 1995, hereafter SMOK95).

3.3. *Results of the DEM Analysis*

The DEM inversion procedure results in a minimum $\chi^2 = 858$ [with 41 temperature intervals and 926 wavelength bins the number of degrees of freedom (dof) is 885], which is essentially a perfect fit for the assumed errors as given by Poisson counting statistics. The fit residuals are nowhere larger than 3 σ and we found no evidence for systematic tendencies, in the sense of the fit residuals being systematically above or below zero in certain wavelength ranges (except for small feature around 430 Å). The resulting $\boldsymbol{D}$ is plotted in Figure 4 as a solid line with error bars and the corresponding best-fit spectrum is shown in Figures 1–3 by the thick solid line. We note that, because our method is in principle a linear decomposition method, it does not prevent $\boldsymbol{D}$ from taking negative values. In a good fit such negative excursions should be mostly statistically consistent with zero or compensated by neighboring positive values (see, e.g., regions "C" and "D" in Fig. 4), or else removed by applying stronger regularization constraints. These effects are caused by statistical fluctuations in the background-subtracted spectrum which can also show negative counts, and/or by deficiencies in the spectral model used.

In Table 1 we present the accumulated counts during the total exposure predicted by the best-fit DEM model and the DEM region where the lines are formed. These counts are given for the stronger lines labeled in Figures 1–3 and for the

TABLE 1

SPECTRAL LINES INDICATED IN FIGURES 1–3

Ion	Band	λ(Å)	Counts	T region
Ne VIII (Ne VIII blend)	SW	88.09	16	B(0.4), C(0.6)
Ne VII		88.13	11	B
Fe XVIII		93.92	150	C
Ne VII (Ne VIII blend)		97.50	12	B
Fe XXI		97.88	15	C
Ne VIII		98.12	12	B(0.4), C(0.6)
Ne VIII		98.26	24	B(0.4), C(0.6)
Fe XIX		101.55	46	C
Fe XXI (Fe XXI blend)		102.22	37	C
O VIII		102.47	27	C
Fe XVIII		103.94	63	C
Fe XIX		108.37	118	C
Fe XIX		109.97	23	C
Mg VI (Fe XIX blend)		111.56	5	B
Fe XIX		111.70	17	C
Ni XXIII		111.86	7	C
Fe XXII		114.41	22	C
Ne VII (Fe XXII blend)		116.69	15	B
Fe XXII		117.17	114	C
Fe XXI		117.51	26	C
Fe XX		118.66	48	C
Fe XIX		120.00	25	C
Fe XX		121.83	82	C
Fe XXI		128.73	125	C
Fe XXIII (Fe XXIII blend)		132.85	143	C
Fe XX		132.85	82	C
Fe XXII		135.78	73	C
Fe XXIV	MW	192.02	41	C(0.4), D(0.6)
Fe XXIV (He II blend)		255.09	12	C(0.4), D(0.6)
He II		256.32	23	A(0.9), C(0.1)
S XIII		256.66	16	C
Fe XV		284.15	32	C
He II		303.78	392	A
Fe XVI		335.41	43	C
Fe XVI	LW	360.80	27	C
Ne VII		465.22	15	B
O III		507.68	20	A
Continuum	SW	76–100	1160	C(0.25), D(0.75)
Continuum		100–120	940	C(0.25), D(0.75)
Continuum		120–180	860	C(0.25), D(0.75)

NOTE.—Counts: predicted model counts for total exposure. T region: temperature region(s) of the DEM (see Fig. 5) where the line or continuum is formed (in parentheses the relative contribution to the line or continuum strength).

SW continuum in various broad bands. We distinguish four different regions in the $\boldsymbol{D}(T)$ plot: A, B, C, and D (see Fig. 4).

1. At temperatures below about 10^5 K (region "A") a "chromospheric" component is seen that is predominantly determined by the strong helium II line at 304 Å and (upper limts of) a few other, weaker lines (e.g., He II 256 Å and O III 507 Å). The strong He II 304 Å line is certainly optically thick, so that the $\boldsymbol{D}(T)$ at these temperatures should be regarded only as a formal, certainly not unique solution.

2. There is very little emission from plasma between 10^5 K and 2×10^6 K (region "B"). The striking absence of emission in this region is also found for other active cool stars such as α Aur and ξ UMa (see SMOK95).

3. Most of the lines in the spectrum of AB Dor (Figs. 1–3) are due to various ions of iron from Fe XV up to Fe XXIV, forming at temperatures from about 2.5×10^6 K up to $\sim 1.6 \times 10^7$ K. This corresponds to region "C" between 2×10^6 K and 10^7. The pronounced emission in this region shows some indication of a temperature substructure with two peaks around about 3×10^6 K and 10^7 K, but which are barely resolved at the intrinsic temperature resolution of typically a factor of 2 (determined by the width of the temperature interval over which most lines contribute to the spectrum, which in turn reflects the ionization and excitation balance). The total emission measure $EM = n_e n_H V$ for this region is 3×10^{52} cm^{-3}.

4. Finally, in region "D" the formal $\boldsymbol{D}(T)$ solution shows a strong component above about 2.0×10^7 K as a high-temperature "tail," which reflects the presence of a featureless continuum in, foremost, the SW spectrum (see Fig. 1), but which depends on the model used to fit the data. This high-temperature component appears to be a common feature in the formal DEM solutions for many other cool stars, except for the solar-like star χ^1 Ori, while for the quiet Sun itself such a hot component is never detected (MKSOA95; SMOK95). As indicated in § 3.2, however, the shape of the hot component is not unique, and the *EUVE* data can be used only to show the presence of some hot component under the conditions that the assumptions behind our model are valid (see next section). However, simultaneous *ASCA* observations of AB Dor do not show any extraordinary hot component (see White et al. 1995b) and thus seem at first sight to contradict our *EUVE* results. Therefore the presence of the high-temperature component deserves a special attention.

3.4. *Is the High-temperature Component Real?*

The SW continuum is found in the *EUVE* spectra of many cool stars and its interpretation is therefore an important issue in the analysis of *EUVE* data. It appears to be a genuine hot component, but a component as strong as shown in Figure 4 is inconsistent with X-ray spectra of these stars. Mewe and coworkers have discussed various explanations of this feature (MKSOA95; SMOK95), and we summarize their findings here. They rule out the possibility that it is a background feature, since the detector background has quite different characteristics and the continuum has a flat spectrum consistent with genuine plasma emission. The flat spectrum rules out the possibility that it is an optically thick component. The two most likely explanations are that the abundances in the stellar corona are not the solar photospheric abundances which we have assumed, or else the emitting region is an asymmetric, optically thick but effectively thin plasma in which the photons of the stronger lines are resonantly scattered and destroyed upon impact on the lower chromosphere.

In an asymmetric atmosphere, where—at least on average—the emitting plasma lies closer to the photosphere than the plasma that resonantly scatters line photons, the line-to-line and line-to-continuum ratios can be modified from what is expected from a purely optically thin plasma. Upward-traveling photons which are scattered downward will be absorbed in the photosphere or chromosphere, and the loss of these upgoing photons is only partly compensated by upward scattering of initially downward-traveling photons, owing to the asymmetry (see Schrijver, van den Oord, & Mewe 1994 for details). A direct method to test the possibility that the stellar corona is marginally optically thick in some spectral lines is based on a direct analysis of the relative strengths of the observed lines. For example, Dupree et al. (1993) studied in detail the intensity ratios of the strongest lines around 100 Å in the spectrum of the bright source α Aur (which had a high signal-to-noise ratio) for which the intensities are predicted by known branching ratios. They show that the observed and

predicted line ratios do in fact agree fairly well, which is consistent with the absence of significant line-photon scattering in the corona of this source. However, in the case of AB Dor the lower signal-to-noise ratios of the lines do not permit such a detailed analysis.

The alternative interpretation of the SW continuum is that its strength relative to the (predominantly Fe) line emission is due to a lower-than-assumed Fe abundance, rather than the presence of very hot plasma. Lowering the abundance of an element reduces the line-to-continuum ratio, because the line excitation is proportional to the product $n_i n_e$ of the number densities of the emitting ion, n_i, and of the exciting electrons, n_e, whereas the continuum emission is predominantly free-free emission and free-bound emission, dominated by the recombination with hydrogen (both proportional to the product $n_e n_H$). The line-to-continuum ratio therefore varies proportionally to the element's abundance.

There is independent evidence that the Fe abundance is lower than the cosmic fraction which we initially assumed. A preliminary two-temperature fit to the *ASCA* spectra using the MEKA model with variable abundances yields the following parameters for the two components (White et al. 1995b; R. Pallavicini 1994, private communication): $T_1 = 7 \times 10^6$ K, $EM_1 = 8 \times 10^{52}$ cm^{-3}, $T_2 = 1.7 \times 10^7$ K, $EM_2 = 9 \times 10^{52}$ cm^{-3}, with the low-temperature component similar to component "C" of the *EUVE* results. Most importantly, the *ASCA* data suggests a low iron abundance, in both components (i.e., relative to solar: $A_{Fe_1} = 0.35 \pm 0.08$ and $A_{Fe_2} = 0.133 \pm 0.04$). Furthermore, the results yield an underabundance of a factor 3–4 for most of the medium-Z elements except neon. We have therefore investigated the effect of varying abundances on our DEM solutions. A DEM fit allowing the iron abundance to vary yields a best-fit value of 1.1 ± 0.4. Figure 4 (*dashed line*) shows the DEM distribution resulting from an assumed iron abundance of 0.3 (i.e., 2 σ below the best-fit value). As expected, the emission measure for the relatively cooler component in region "C" is increased in order to generate the observed iron line fluxes. The hottest component "D" is reduced in strength, but it does not completely vanish, however.

Motivated by these results we carried out a DEM fit using for the Fe abundance the low value of 0.133 corresponding to the hottest component of the *ASCA* model. The resulting DEM is shown in Figure 5. Again as expected the emission measure of region "C" is increased, but now the hot component "D" is statistically insignificant! The fit is still acceptable ($\chi^2 = 897$), although formally this low iron abundance of 0.133 is inconsistent with the error limits derived before, based on the χ^2-statistic. However, the regularization method used in our DEM analysis causes χ^2 to increase typically by $\sqrt{2 \times \mathrm{dof}} \approx 42$ as compared to an unregularized fit. Since however the DEM with solar abundances is significantly different from the DEM with the adopted *ASCA* abundances, we need in principle to apply different regularizations in the two fits; in fact, as long as any two different models have χ^2-values that differ by less than ~ 42 and are both statistically acceptable, we cannot discriminate between these models based solely upon our DEM analysis. Since in our case the best-fit χ^2-values differ by 39, both the solar-abundance model and the *ASCA*-abundance model are acceptable.

Further, if we simulate an *EUVE* spectrum using the *ASCA* model and then analyze this with our DEM program using *solar* abundances, we obtain a DEM which contains a high-temperature component similar to that deduced from the observed *EUVE* spectrum, but if we fit the simulated spectrum using the (generally lower) *ASCA* abundances the hot component is suppressed.

These results emphasize the important role which abundances play in modeling the DEM from *EUVE* observations. Because the DEM above 2×10^7 K is so poorly constrained, it is very difficult to determine the Fe abundance in a hot corona from the *EUVE* spectrum alone; some independent measurement of abundances is required. Fortunately, *ASCA* is well suited for the measurement of abundances in hot coronae, and will provide abundance information for many *EUVE* sources. Derivation of abundances (e.g., iron and neon) from the combined *ASCA*/*EUVE* data will be presented by Mewe et al. (1995b).

4. DISCUSSION AND CONCLUSIONS

Virtually all studies of the X-ray emission from stellar coronae have required that multitemperature distributions be present in order to obtain adequate fits to the data, e.g., Swank et al. (1981) using the *Einstein* Solid State Spectrometer, Majer et al. (1986) and Schmitt et al. (1990) using the pulse height spectra of the *Einstein* IPC, Mewe et al. (1982) using the objective grating spectra from *Einstein*, Pasquini, Schmitt, & Pallavicini (1988) who studied *EXOSAT* ME-detector spectra, and Lemen et al. (1989) who studied transmission-grating spectra from *EXOSAT*. DEM derived from broadband measurements have often been questioned as possibly either instrumental in origin, or else due to detectors with poor spectral-line diagnostic capabilities. In this context, the *EUVE* spectra are very important as the DEM-diagnostics are based on different spectral lines arising in a broad temperature range, as was the case with the transmission-grating *EXOSAT* spectra, but for higher temperatures.

The differential emission measure distribution derived from our observations which, as noted above, were taken during a relatively low-activity state has the following properties (see Fig. 4):

1. There is plasma present at temperatures below about 10^5 K (region "A") whose contribution to the DEM solution is for a large part determined by the strong (and optically thick) He II 304 Å line. However, the error bars are large and the optical thin model is not appropriate to describe the He II emission so that no conclusions can be drawn about the DEM below about 10^5 K (perhaps it should be considered only as a lower limit).

2. A striking feature is the nearly complete absence of plasma in the region ("B") between about 10^5 K and 2×10^6 K which spans more than one decade in temperature. This is consistent with the absence of any strong line emission in the LW band formed at these temperatures.

3. The dominant component, responsible for all pronounced Fe XIX to Fe XXIII lines, part of the SW continuum, and the Fe XXIV lines, occurs in region "C" between about 2×10^6 K and 2×10^7 K. If we assume the low Fe abundance, it produces the whole continuum and then the total emission measure is $\simeq 1.6 \times 10^{53}$ cm^{-3}.

4. Finally, the formal DEM solution shows a high-temperature component ("D") extending from $\sim 2 \times 10^7$ K up to 10^8 K, which is needed to fit most of the observed continuum emission in the SW band and partly also the Fe XXIV lines *if* solar abundances are assumed. At first sight such a component seems to be in conflict with the *ASCA* observations,

which show no evidence for such a hot plasma. However, if we reduce the iron abundance by a factor of 7, the hot component vanishes (see Fig. 5) and the *EUVE* data can be reconciled with the *ASCA* data.

It is interesting to compare these results with those from the analysis of the *EUVE* spectra of other cool stars, either solar-like single stars or components of RS CVn-like binaries. The *EUVE* spectrum of AB Dor looks quite similar to the spectra of, e.g., the RS CVn type stars α Aur (Dupree et al. 1993; SMOK95) and ξ UMa (SMOK95), and of the active M dwarf AU Mic (Monsignori Fossi & Landini 1994; SMOK95), but it looks different from the spectra of the solar-type star χ^1 Ori (Haisch, Drake, & Schmitt 1994; SMOK95), of α Cen (MKSOA95), of α CMi (Drake, Laming, & Widing 1995; SMOK95), and of the active RS CVn type star HR 1099 (Brown 1994), σ Gem (SMOK95), and AY Cet (SMOK95). For example, the DEM of AB Dor does share properties in common especially with α Aur, ξ UMa, and AU Mic.

We are grateful to the EGO personnel, in particular to A. Wiercigroch, for help with spectral reductions and to J. M. Braun for assistance in preparing the figures.

S. M. R. research has been supported by a grant from the Natural Sciences and Engineering Research Council of Canada. J. S. K. and R. M. acknowledge support from the Space Research Organization of the Netherlands (SRON). S. M. W. gratefully acknowledges support from *EUVE* Guest Investigator grant NAG-5-2364 and from NSF grant AST 92-17891. We are grateful to an anonymous referee for valuable comments and R. M. and J. S. K. are indebted to G. H. J. van den Oord and C. J. Schrijver for many discussions which helped to improve the paper substantially.

REFERENCES

Anders, E., & Grevesse, N. 1989, Geochim. Cosmochim. Acta, 53, 197
Beasley, A. J., & Cram, L. E. 1993, MNRAS, 264, 570
Brown, A. 1994, in ASP Conf. Ser. 64, Cool Stars, Stellar Systems, and the Sun, Eighth Cambridge Workshop, ed. J.-P. Caillault (San Francisco: ASP), 23
Collier, A. C. 1982, MNRAS, 200, 489
Collier Cameron, A., Bedford, D. K., Rucinski, S. M., Vilhu, O., & White, N. E. 1988, MNRAS, 231, 131
Craig, I. J. D., & Brown, J. C. 1986, Inverse Problems in Astronomy (Bristol: Adam Hilger Ltd.)
Drake, J. J., Laming, J. M., & Widing, K. G. 1995, ApJ, 443, 393
Dupree, A. K., Brickhouse, N. S., Green, J. C., & Raymond, J. C. 1993, ApJ, 418, L41
EUVE Guest Observer Handbook. 1993 (NRA 93-OSSA-X)
Haisch, B., Drake, J., & Schmitt, J. H. M. M. 1994, ApJ, 421, L39
Innis, J. L., Thompson, K., & Coates, D. W. 1986, MNRAS, 223, 183
Kaastra, J. S., & Mewe, R. 1993, Legacy, 3, 16
Kürster, M., Schmitt, J. H. M. M., & Fleming, T. A. 1992, in ASP Conf. Ser. 26, Cool Stars, Stellar Systems, and the Sun, ed. M. S. Giampapa & J. A. Bookbinder (San Francisco: ASP), 109
Landini, M., & Monsignori Fossi, B. C. 1990, A&AS, 82, 229
Lemen, J. R., Mewe, R., Schrijver, C. J., & Fludra, A. 1989, ApJ, 341, 474
Lim, J., Nelson, G. J., Castro, C., Kilkenny, D., & van Wyk, F. 1992, ApJ, 388, L27
Lim, J., White, S. M., Nelson, G. J., & Benz, A. O. 1994, ApJ, 430, 332
Majer, P., Schmitt J. H. M. M., Golub, L., Harnden, F. R., & Rosner, R. 1986, ApJ, 300, 360
Mewe, R., et al. 1982, ApJ, 260, 233
Mewe, R., Gronenschild, E. H. B. M., & van den Oord, G. H. J. 1985, A&AS, 62, 197
Mewe, R., & Kaastra, J. S. 1994, European Astron. Soc. Newsletter, 8, 3
Mewe, R., Kaastra, J. S., Schrijver, C. J., van den Oord, G. H. J., & Alkemade, F. J. M. 1995a, A&A, in press (MKSOA95)
Mewe, R., Kaastra, J. S., Pallavicini, R., & White, S. M. 1995b, in preparation
Mewe, R., Lemen, J. R., & van den Oord, G. H. J. 1986, A&AS, 65, 511
Monsignori Fossi, B. C., & Landini, M. 1994, A&A, 284, 900
Pakull, M. W. 1981, A&A, 104, 33
Pasquini L., Schmitt J. H. M. M., & Pallavicini, R. 1988, in Activity in Cool Star Envelopes, ed. O. Havnes, B. R. Petterson, J. H. M. M. Schmitt, & J. E. Solheim (Dordrecht: Kluwer), 241
Press, W. H., Flanner, B. P., Teukolsky, S. A., Vetterling, W. T. 1992, Numerical Recipes (Cambridge: Cambridge Univ. Press)
Rucinski, S. M. 1982, Inf. Bull. Var. Stars, 2203
———. 1985, MNRAS, 215, 591
Rumph, T., Bowyer, S., & Vennes, S. 1994, AJ, 107, 2108
Schmitt, J. H. M. M., Callura, A., Sciortino, S., Vaiana, G. S., Harnden, F. R., & Rosner, R. 1990, ApJ, 365, 704
Schrijver, C. J., Mewe, R., van den Oord, G. H. J., & Kaastra, J. S. 1995, A&A, in press (SMOK95)
Schrijver, C. J., van den Oord, G. H. J., & Mewe, R. 1994, A&A, 289, L23
Swank, J. H., White N. E., Holt, S. S., & Becker, R. H. 1981, ApJ, 246, 208
Sylwester, J., Schrijver, J., & Mewe, R. 1980, Solar Phys., 67, 285
Verner, D. A., Yakovlev, D. G., Band, I. M., & Trzhaskovskaya, M. B. 1993, Atomic Data Nucl. Data Tables, 55, 233
Vilhu, O., Ambruster, C. W., Neff, J. E., Linsky, J. L., Brandenburg, A., Ilyinn, I. V., & Shakhovskaya, N. I. 1989, A&A, 222, 179
Vilhu, O., Gustafsson, B., & Edvardson, B. 1987, ApJ, 320, 850
Vilhu, O., & Linsky, J. L. 1987, PASP, 99, 1071
Vilhu, O., Tsuru, T., Collier Cameron, A., Budding, E., Banks, T., Slee, O. B., Ehrenfreund, P., & Foing, B. H. 1993, A&A, 278, 467
Vilhu, O., & Walter, F. M. 1987, ApJ, 321, 958
White, S. M., Lim, J., Rucinski, S., Roberts, G., Ryan, S., Prado, P., Kilkenny, D., & Kundu, M. R. 1995a, in preparation
White, S. M., Pallavicini, R., & Lim, J. 1995b, in preparation